Lu et al., J Geol Geophys 2018, 7:1
DOI: 10.4172/2381-8719.1000320

Journal of Geology & Geophysics
ISSN: 2381-8719

Research Article Open Access

U-Pb Detrital Zircon Geochronology of Late Triassic to Early Jurassic Sandstones in the Northwestern Junggar Basin and its Implications

Xinchuan Lu[1,2*], Xiangyang Xie[2], Shuncun Zhang[1], Arthur B Busbey[2], Shengyin Zhang[1], Shekuan Du[1], Guoqiang Sun[1] and Jian Shi[1]

[1]*Key Laboratory of Petroleum Resources, Gansu Province / Key Laboratory of Petroleum Resources Research, Institute of Geology and Geophysics, Chinese Academy of Sciences, Lanzhou 730000, Gansu Province, PR China*

[2]*School of Geology, Energy, and Environment, Texas Christian University, Fort Worth, TX -76129, USA*

Abstract

The Junggar Basin is a Late Carboniferous foreland basin in northwestern China surrounded by different mountain belts. The west Junggar Basin has a complicated tectonic history with multiple subduction and collision events that controlled sedimentation and basin development. In this study, absolute dating of igneous rocks, rock geochemistry, and U-Pb detrital zircon geochronology were used to document the provenance of the Triassic-Jurassic clastic rocks in the northwest margin of Junggar Basin and determine local sources and tectonic setting. Granitic zircons with the youngest concordia age reveal the north Karamay pluton was formed at 292.6 ± 0.7 Ma, suggesting that they are post-collision granites. Late Triassic-Lower Early Jurassic strata were derived from Zhayier Mountain south of the Darbute fault. Starting with the Upper Early Jurassic Sangonghe Formation-Lower Middle Jurassic Xishanyao Formation, the strata changed from a single source to mix multiple sources. Sediment sources are widespread, including the northern Karamay granitic plutons, the area north of the Darbute fault, with potentially minor contributions from the southern margin of the Junggar Basin.

Keywords: U-Pb dating; LA-ICP-MS; Provenance; Junggar Basin

Introduction

The Central Asian Orogenic Belt (CAOB) is a typical pacific-type orogenic belt located among the East European, Siberian, North China and Tarim cratons [1] (Figure 1A). As the eastern margin of the Kazakhstan orocline, the western Junggar region provides a unique opportunity for studying the evolution of the CAOB [2]. Previous studies have mainly focused on the Tianshan orogenic belt [3,4], and the Altay orogenic belt and east Junggar tectonic activations [5,6]. Studies have included time of formation and the tectonic history of orogen by using zircon dating and the geochemistry of volcanic rocks or/and the ophiolitic mélange. Recently, there has been a surge of renewed research interests in west Junggar regarding the closing time of the west Junggar ocean, the tectonic evolution of the Junggar ocean and western Junggar, and intra-ocean arc subduction and continental growth [7-12].

The Junggar Basin was a foreland basin in the early Permian following the closure of a branch the Turkestan Ocean [5,13]. The northwestern margin of the Junggar Basin is an important potential area for hydrocarbon exploration and production [14-16]. Provenance studies of Mesozoic to Cenozoic sandstones in the southern Junggar Basin [3,17,18] and the hinterland of the Junggar Basin [19], and northern Junggar Basin geochemistry [20] have important implications in hydrocarbon exploration in the Junggar Basin. However, most efforts have been focused on the tectonic activity of the Tianshan orogenic belt, sedimentary records along the southern margin of basin or strata older than the Carboniferous, while sediment sources in the northwestern margin of Junggar Basin and the potential impact of Tianshan tectonic activity remains less constrained.

In this study, a total of 14 samples were collected from the northwest Junggar Basin near Zhayier Mountain. U-Pb detrital zircon dating, petrology, rock geochemistry and the U-Pb geochronology of igneous rocks were applied to document the provenance of Triassic to Jurassic clastic rocks. Results provide insight into the interaction between basin marginal deformation belts and their control on sedimentary sources along the northwestern Junggar Basin margin.

Geological Settings and Stratigraphy

The Junggar Basin is located in the southwestern part of the CAOB and covers a total area of approximately 136,000 km^2 at the junction of the Kazakhstan, Siberia and Tarim blocks [21-23]. It is a giant intraplate Meso-Cenozoic basin (Figures 1 A and B) [24]. In the Precambrian, this area lay between the Early Paleozoic Altay-Junggar-Ergun collision belt and the Late Paleozoic Tianshan-Hingganling collision belt (the eastern extension of the central Asian orogenic belt) that were controlled by Altay, Junggar-east Kazakhstan and Ili-Balchas tectonics. From the Middle Devonian to the Middle Permian, the Junggar Basin became terrestrial due to the Tianshan activity [25]. The basin is underlain by Paleozoic oceanic crust, accretionary wedges, island-arcs, and Precambrian crystalline basement [26,27]. Carboniferous collisions lead to the formation of mountains and a foreland surrounding the basin with respect to Variscan (Hercynian) collisional episodes in Central Asia [14,28-30]. The juvenile Junggar Basin was formed in the Late Carboniferous after the final collision of the combined Tarim–central Tianshan block with the northern Tianshan block by post-collisional transcurrent tectonics during the Early and Middle Permian and flexural foreland subsidence in the Late Permian when subduction terminated [21]. However, their subsequent development was linked to the re-activation of suture zones during the Cimmerian (Indosinian and Yanshanian) and Himalayan orogenic episodes. The subsidence

***Corresponding author:** Xinchuan Lu, Key Laboratory of Petroleum Resources, Gansu Province/Key Laboratory of Petroleum Resources Research, Institute of Geology and Geophysics, Chinese Academy of Sciences, Lanzhou 730000, Gansu Province, PR China, Tel: + 86-10-68597521; E-mail: xclu@lzb.ac.cn

Received November 20, 2017; **Accepted** December 11, 2017; **Published** December 19, 2017

Citation: Lu X, Xie X, Zhang S, Busbey AB, Zhang S, et al. (2017) U-Pb Detrital Zircon Geochronology of Late Triassic to Early Jurassic Sandstones in the Northwestern Junggar Basin and its Implications. J Geol Geophys 7: 320. doi: 10.4172/2381-8719.1000320

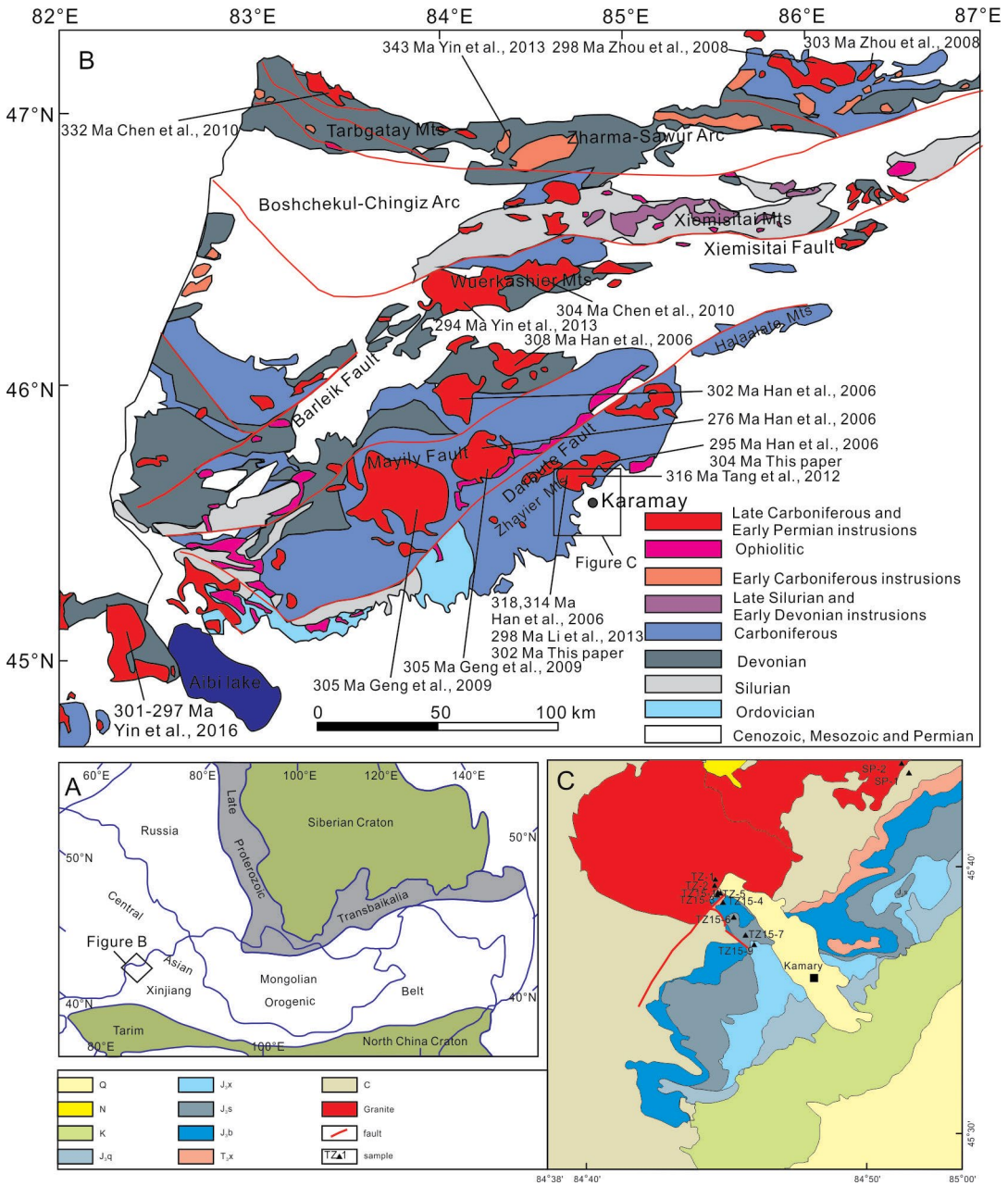

Figure 1: A. Simplified tectonic divisions of the Central Asian Orogenic Belt (after Gao [10]),
B. Simplified geological map of western Junggar Basin (modified after (Xu [55], Yin [59]),
C. Simplified geological map of Karamay (modified after 1:200000 geological map 1965 XBGMR, [50]).

was due to flexural downbowing that depressed the crust under the tectonic load of thrust sheets associated with the uplifted mountain ranges [14,31].

The Karamay collision zone is a series of successive accretionary complexes separated by northwest-southeast oriented uplifts and depressions paralleling suture lines (fault), such as the Darbute and Mayily faults (Figure 1B). The northwest Junggar Basin is bordered by the Karamay thrust belt which was formed by thrusted sequences of Carboniferous rocks (Figures 1 and 2). These boundary faults controlled Permian and Triassic deposition in the northwestern margin of the Junggar Basin, and the Permian and Jurassic strata thickening from basin edge to inner basin (Figure 2). In the northern Junggar Basin, the Zharma-Saur and Boshchekul-Chingiz volcanic arcs consist of late Paleozoic tuffs, tuffaceous limestones and sandstones and early Paleozoic tuffaceous siltstones, tuffaceous sandstones and muddy siltstones, which were intruded between 304 and 263 Ma [32,33]. These plutons reflect the southward subduction of the Irtysh-Zaysan Ocean beneath the Kazakhstan block [34].

Devonian to Carboniferous strata are mainly sandstones and volcanic rocks, including basalt, andesitic basalt and andesite [2]. Reported SHRIMP and LA-ICP-MS U-Pb dates of volcanic intrusions range from 332 to 276 Ma (Figure 1B) [32]. The Carboniferous strata

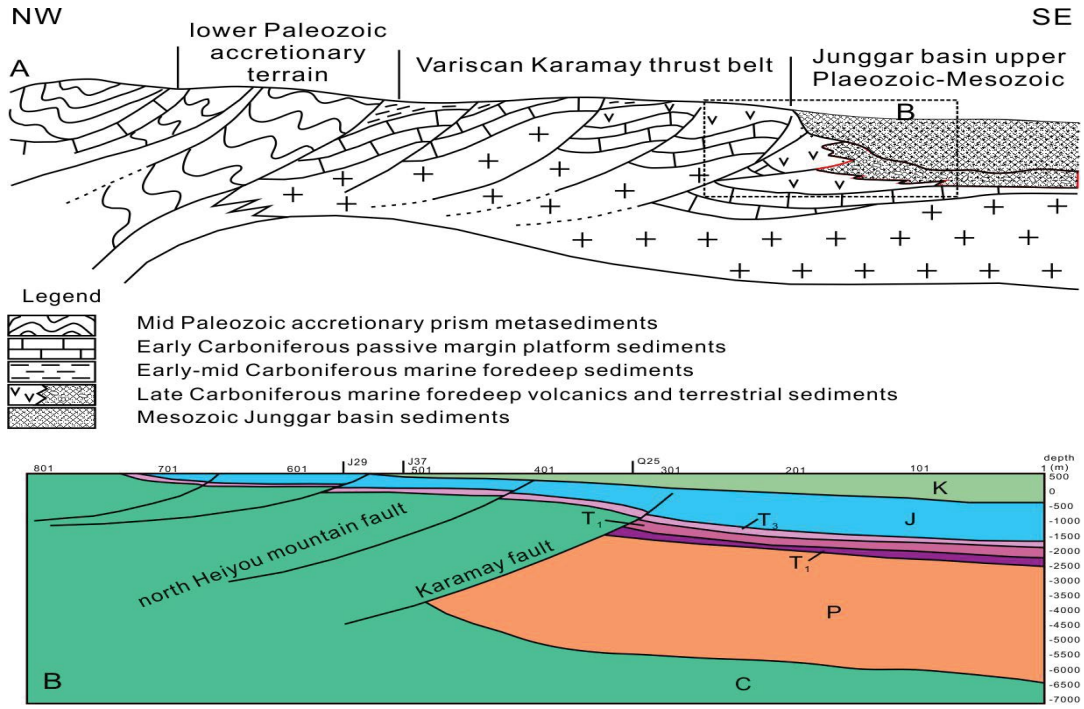

Figure 2: A. Architectural model of the Junggar collision zone (after from Lawrence [2]), **B**. Seismic section interpretation (from an internal report).

are mainly composed of gray-green bedded tuffs and sandstones with intrusive granite bodies. No Permian deposition exists near the Karamay, but it thickens towards the southeast (Figure 2). Lower Permian strata (the Jiamuhe and Fengcheng Formations) consist of grayish conglomerates, sandstones and mudstones with some andesites and tuffs, with considerable dolomite in the Fengcheng Formation (P1f). The middle Permian Xiazijie Formation (P2x) and the Lower Wuerhe Formation (P2w) are mostly comprised of conglomerates and sandstones. The upper Permian Upper Wuerhe Formation (P3w) is mainly composed of conglomerates. Overall, Permian strata generally thin from the northwest to the southeast. The Lower Triassic Baikouquan Formation (T1b) consists of reddish conglomerates, sandstones and mudstones. The Middle Triassic Karamay Formation (T2k) is dominated by conglomerates and sandstones, and the Upper Triassic Baijiantan Formation (T3b), in contrast with the Xiaoquangou Formation in the southern margin, is mainly composed of conglomerates, sandstones and mudstones. The Jurassic strata consist of non-marine conglomerates, sandstones, siltstones, mudstones and coal seams. Among them, the Middle Jurassic Xishanyao Formation (J2x) is composed of dark grayish mudstones with coal seams, oil sandstones and abundant phytolites. Angular unconformities have been observed between P2x and P1f, P2w and P3w, P3w and T1b, T3b and J1b, J3q and K1tg, respectively (Figure 3). From the Permian to the Jurassic, there are alluvial fan facies, fan delta facies and river facies distributed along the northwestern margin of the Junggar Basin [15,35]. In the study area deltaic facies are present in the Triassic and fluvial facies in the Jurassic [36] (Figure 4).

Sampling and Methods

Sampling and sample preparation

All samples were collected from two outcrops ranging in age from the Carboniferous to Paleogene. These are the Tuziakeneigou section northwest of Karamay city and the Sanping section northeast of Karamay city (Figure 1 C). A total of 14 samples were collected, 10 samples of sandstone and conglomerate, granite and tuff were selected for U-Pb zircon geochronology, and eight samples were chosen for trace and rare elements from mudstones, granites and tuffs (Figure 4).

Zircon grains of 10 samples, including one tuff sample (SP-1), three granite samples (TZ-1, TZ-2 and SP-2) and six sandy conglomerate samples (TZ15-1, 3, 4, 6, 7, 9), were extracted from rock samples at Langfang Geoscience Exploration Technology Service Limited in Hebei Province, China. The zircon mineral separation procedures were in the following order: Jaw crusher, disc mill, Wilfley table, and heavy liquid separation [37,38]. A mineral separation process was applied to obtain a full proportional representation of all zircon populations. Mineral separation was initially conducted at <600 μm and then at <420 μm with an additional step of <300 μm for a tuff sample [39]. All zircon grains were mounted in epoxy resin, polished to expose surfaces, and were imaged by a cathodoluminescence (CL) microscope at the Langfang Geoscience Exploration Technology Service Limited in Hebei Province, China. All CL images served as reference maps for locating laser targets mainly in order to avoid older cores, inclusions, and/or fractures. Eight samples were selected, which are TZ-1, TZ-2, TZ-5, TZ-7, SP-1 and SP-2 (used before), TZ-4 from the north Karamay granitic pluton in the Tuziakeneigou section, SP-3 from the granitic pluton in Sanping section, and were crushed by mortar to less than 200 powder mesh to measure the concentration of trace and rare earth elements with an inductively coupled plasma mass spectrometer (ICP-MS).

U-Pb LA-ICP-MS analysis

U-Pb single grain isotope analyses were obtained using a laser ablation (Photon-machines Analyte Exite 193 nm) inductively coupled

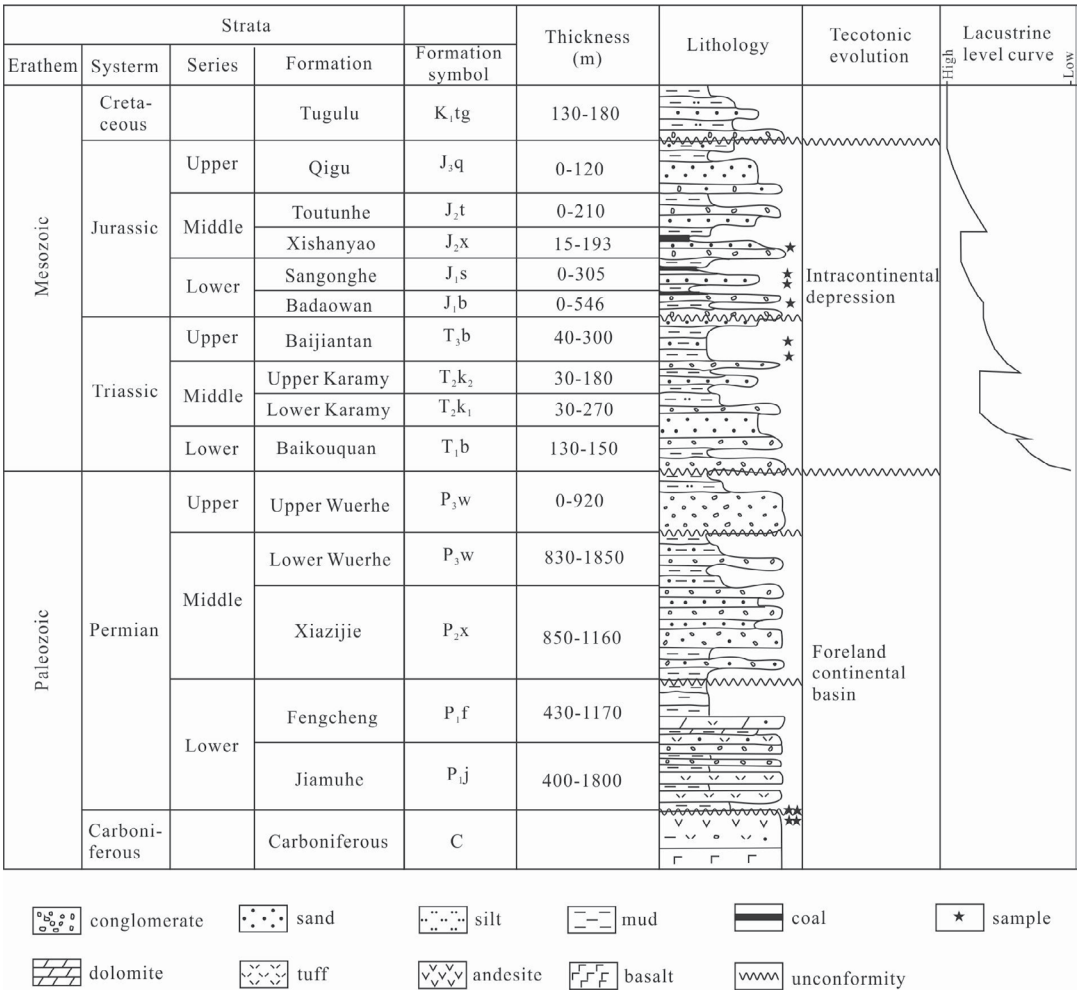

Figure 3: Stratigraphic column of the northwestern Junggar Basin (modified from (Jin [20], Lu [31], Yu [60]).

plasma mass spectrometer (Nu Attom) (LA-ICP-MS) at the Public Technical Service Center, Lanzhou Center for Oil and Gas Resources, Institute of Geology and Geophysics, Chinese Academy of Sciences. Data acquisition involved 30 s of background measurement followed by 30 s of detrital sample ablation in a He/Ar (+N) atmosphere using a laser beam diameter of 25 μm for detrital zircons and 20 μm for volcanic zircons. Sites for analyses were chosen randomly, but avoided inclusions, cracks, and possible contamination. Additionally, when core rim structures were present, only the cores were measured because most rims were too narrow to be analyzed. Mass bias and U-Pb fractionation were corrected using primary standard samples (91500 and GJ-1). The isotopic ratios and elemental concentration of zircons were calculated using ICPMSDataCal (Version 10.9) (Liu et al., 2009). For analyzed detrital zircon grains, 206Pb/238U ages were used for grains younger than 800Ma, and 207Pb/206Pb ages were used for grains older than 800Ma. For zircon ages less than 400Ma, we directly used the 206Pb/238U age. All grain ages within 400-800Ma with >20% discordance and grains younger than 1000 Ma with <5% reverse discordance were discarded [40], as were grains with >10% analytical error, but volcanic zircon data used discordance <40%. All diagrams were produced using the Isoplot V3.0 program of Ludwig [41].

Trace elements and rare earth elements (REE) analysis

About 50 mg of powder (200 mesh) of sample was put in Savillex screw-top Teflon beakers, moistened with a drop of ultra-pure water, and then 1 ml HNO_3 and 3 ml of HF were added. These samples in beakers were digested using this procedure: ultrasonic treatment, evaporation, re-solution with ultra-pure water, additional of 5% HNO_3, heating at 105℃ 72 h, and evaporation on a hot plate to absolutely dissolution. Finally, the solution was transferred to a 100 ml polyethylene bottle and was analyzed by ICP-MS for trace elements and REE using a Nu Attom high precision ICP-MS in the Key Laboratory of Petroleum Resources Research, Institute of Geology and Geophysics, Chinese Academy of Sciences, Lanzhou, China. Relative uncertainties of measurements are better than 5%. Sample preparation and detail analytical procedures are in Lin [42].

Results

Representative Cathodoluminescence (CL) images of analyzed zircons, coupled with their corresponding ages, are illustrated in Figures 5 and 6, Supplementary material. Most zircon grains are euhedral to subhedral. Most show well-developed oscillatory zoning, while only small portion exhibit complex internal structures (Figure 5).

U-Pb zircon dating

The U-Pb detrital zircon data in this study are shown in Figure

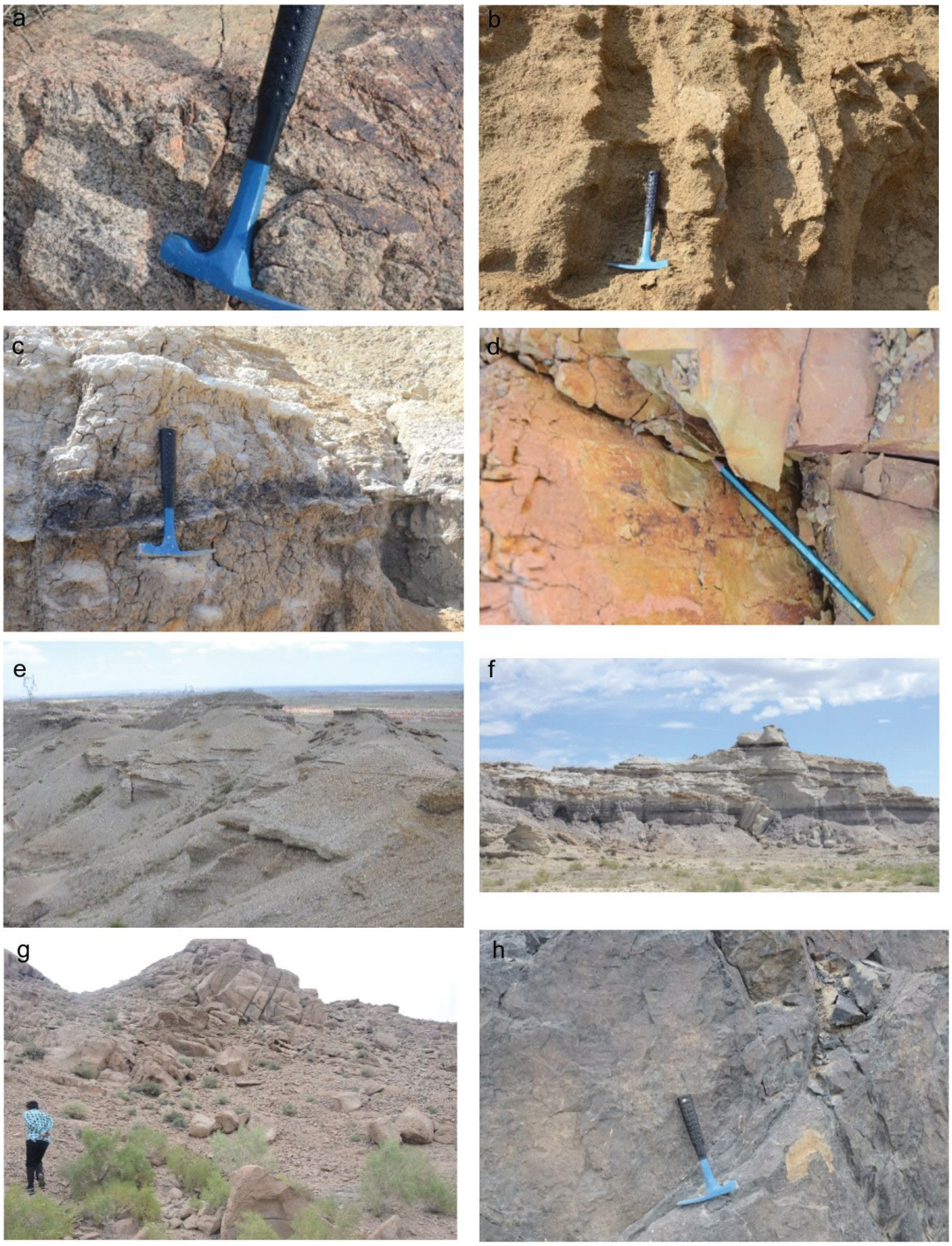

Figure 4: Outcrops of sampling sites in northwestern Junggar Basin.
(a) Sample TZ-1: granite; **(b)** Sample TZ15-1: greyish yellow coarse sandstone; **(c)** Sample TZ15-3: Triassic oil sandstone of the Baijiantan Formation; **(d)** Sample TZ-5: Triassic clay of the Baijiantan Formation; **(e)** Sample TZ15-4: fluvial facies sandstone-conglomerate of the Jurassic Badaowan Formation; **(f)** Sample TZ15-6, TZ15-7 and TZ15-9: Jurassic Sangonghe and Xishanyao Formations, braided river facies; **(g)** Sample SP-3: granite; **(h)** Sample SP-1 tuff; from a to f belong to the Tuziakeneigou section, and **(g)** and h are from the northern Sanping section.

6 and listed in Supplementary material. In total, detrital zircon U-Pb geochronology yielded 823 concordant ages from 853 single grain analyses. Three granitic zircon U-Pb ages were derived statistically from 373 points from 384 analyzed zircon grains. Ages of these zircon grains range from 239 ± 3 to 920 ± 31 Ma.

U-Pb detrital zircon dating

Sample TZ15-1 is a coarse yellow sandstone sample collected from Triassic outcrops. A total of 108 out of 120 single zircon grains yielded ages with less than 20% discordance. Ages of these zircon grains range

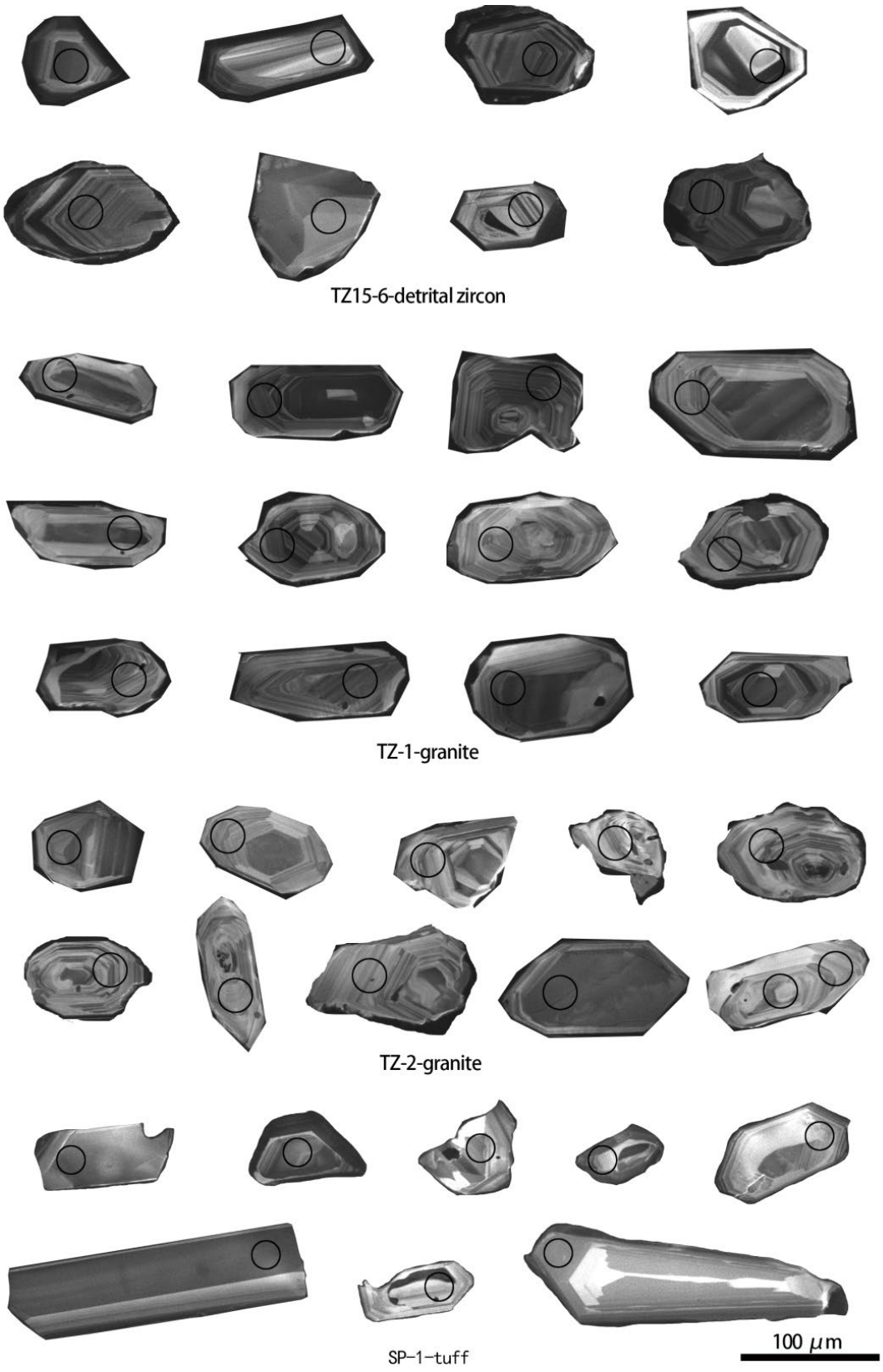

Figure 5: Representative cathodoluminescence (CL) images of detrital zircons. Circles show analytical laser spots.

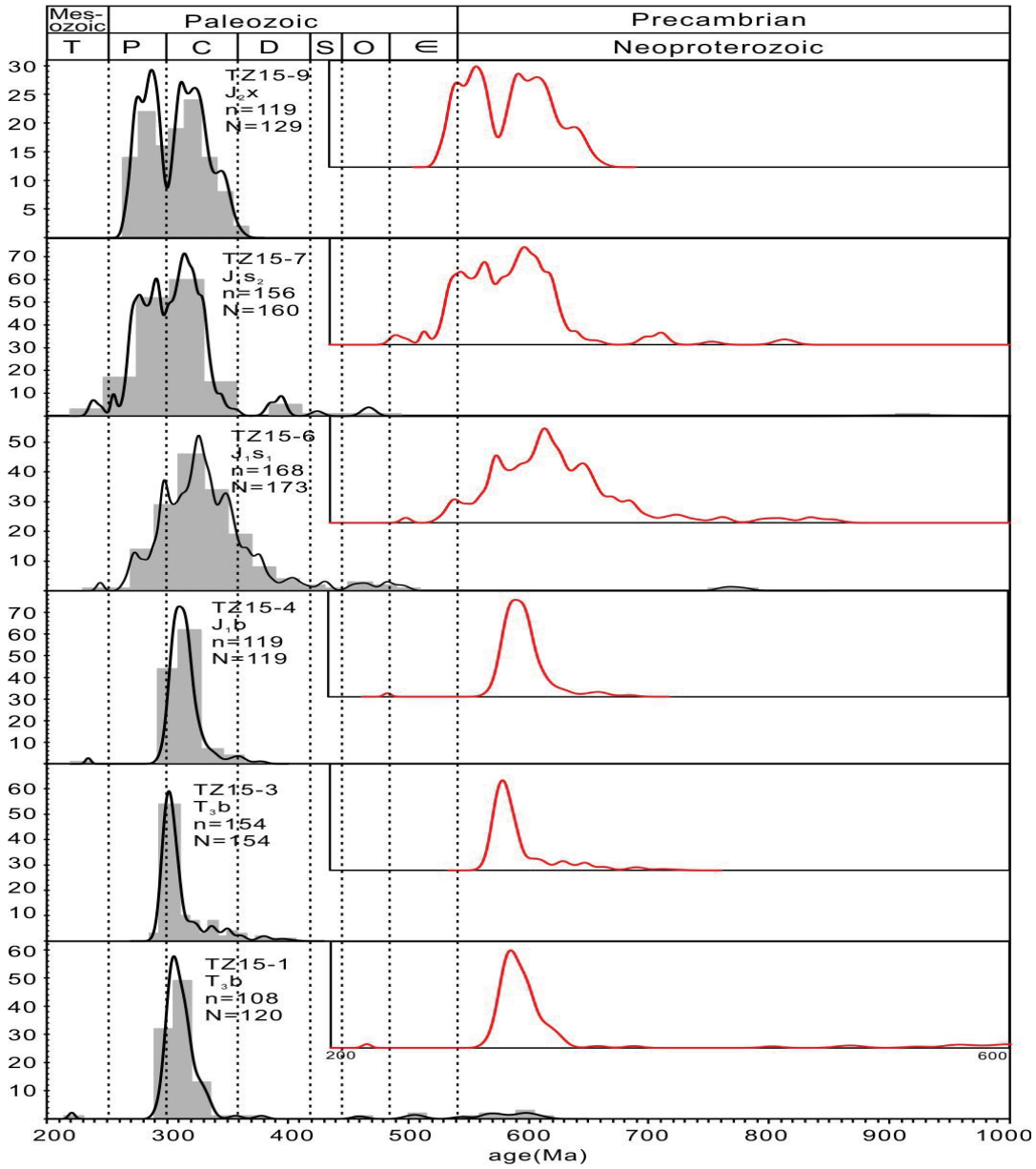

Figure 6: Zircon U-Pb probability density distribution plots. The gray histogram represents the sample number and the black curves the relative probability of zircon ages from 200 to 1000 Ma, the red curve from 200 to 600 Ma.

from 291 ± 4 Ma to 610 ± 9 Ma with a major peak at ~305 Ma and several minor age peaks clustered at ~506, ~570, and 600 Ma. The majority of grains fall within a 291-336 Ma age range (~88%), and the rest belong to a 594-610 Ma age group (~6%).

Sample TZ15-3 is a pebbly sandstone sample collected from the Triassic Baijiantan Formation (Figure 1 C). The ages of 154 zircon grains range from 292 ± 4 Ma to 400 ± 7 Ma with major peak at ~302 Ma and minor clusters at ~321, ~336, ~350, and ~378 Ma. The majority of grains cluster in a 292-317Ma age group (~79%), with the rest belonging to a 318-400Ma age group (~21%).

Sample TZ15-4 is a coarse sandstone sample collected from the Jurassic Badaowan Formation. Ages of 118 zircon grains range from 295 ± 4 Ma to 377 ± 5 Ma with a major peak at ~310 Ma and a minor cluster at ~358 Ma. The majority of grains cluster in a between 295-341 Ma age group (96%).

Sample TZ15-6 is oil sandstone collected from the Jurassic Lower Sangonghe Formation (J_1s^1). The ages of 168 grains, out of 173 single grains, range from 244 ± 3 to 777 ± 8 Ma with major peaks in a ~265-387 Ma age group (90%) with several secondary peaks at ~275, ~298, ~326, ~350 Ma, and minor age peaks at ~406 Ma (2%), ~433 Ma (1%), ~483 Ma (4%), and ~769 Ma (1%).

Sample TZ15-7 is sandstone stained with black oil collected from

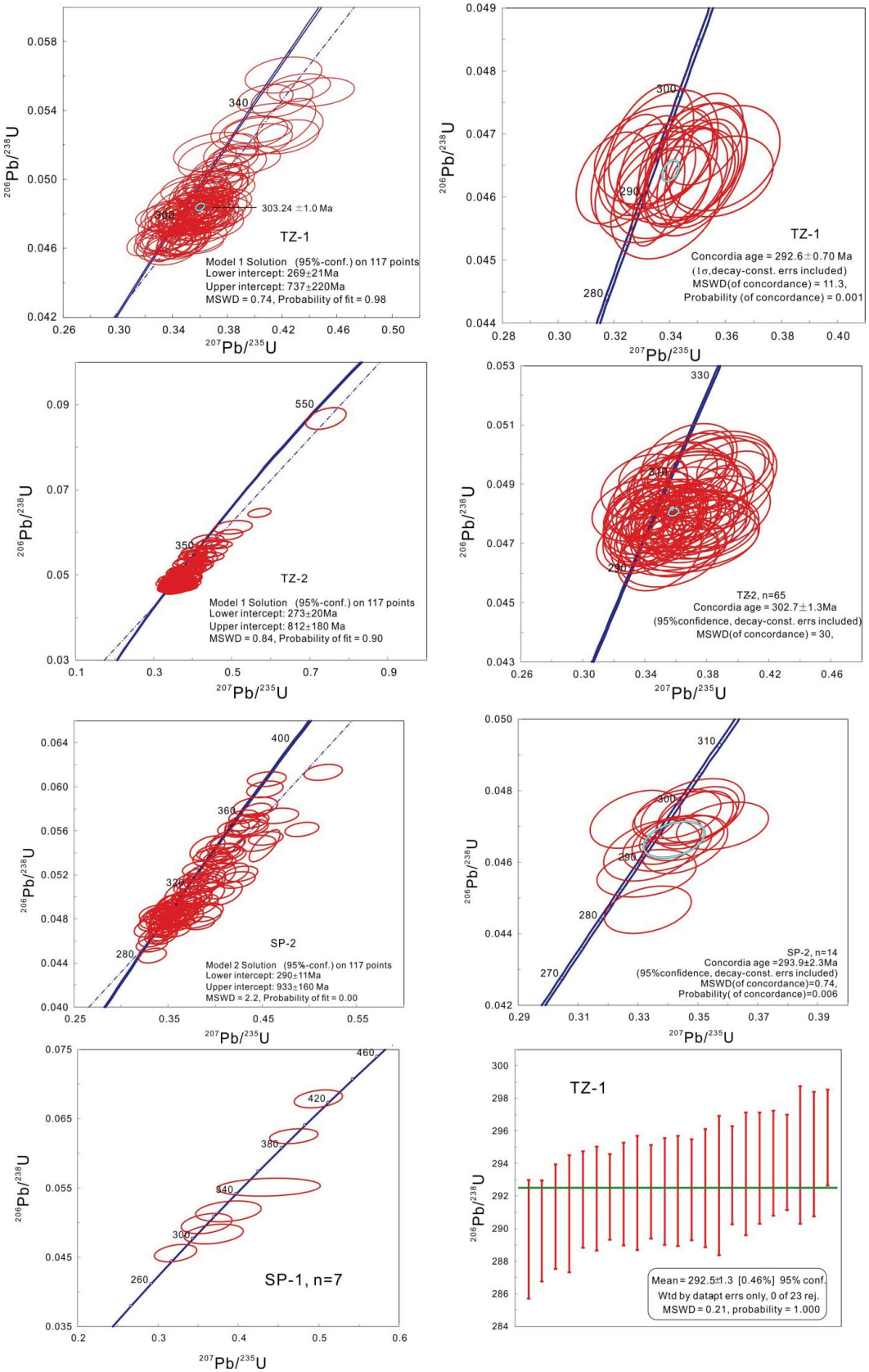

Figure 7: Zircon U-Pb concordia age diagrams for volcanic rock in the Tuziakeneigou and Sanping sections from the northwestern margin of the Junggar Basin.

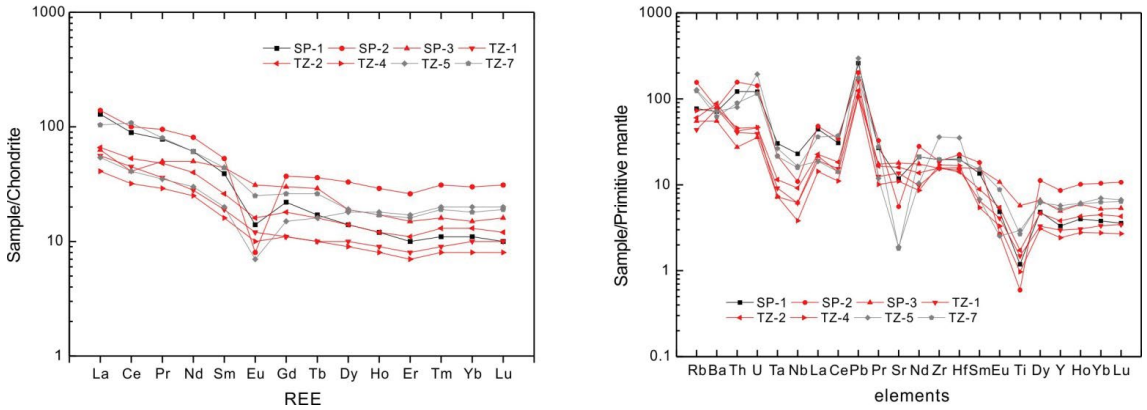

Figure 8: Chondrite-normalized REE distribution patterns **(a)** primitive mantle-normalized multi-element spider diagrams **(b)** (chondrite data and primitive mantle data after Sun and McDonough [39]).

Sample	SP-1	SP-2	SP-3	TZ-1	TZ-2	TZ-4	TZ-5	TZ-7
Lithology	Tuff	Granite	Granite	Granite	Granite	Granite	Mudstone	Mudstone
Ti	1549.5	775.2	7425.0	1932.5	2245.6	1263.2	3811.2	3476.4
Rb	48.8	98.9	34.9	27.6	38.2	46.4	80.7	78.5
Sr	248.1	117.8	379.8	289.0	336.1	231.4	39.9	38.2
Y	15.1	39.1	22.6	13.5	17.4	11.0	26.0	23.7
Zr	219.2	210.7	174.3	172.9	176.0	190.4	402.2	220.7
Nb	16.4	7.8	4.4	4.4	6.5	2.7	11.7	11.3
Mo	0.5	0.9	0.2	0.9	0.9	0.5	1.8	0.6
In	0.1	0.1	0.7	0.1	0.1	0.1	0.2	0.2
Sn	3.5	6.0	32.4	2.3	2.2	1.6	7.6	4.4
Sb	0.1	0.1	0.2	0.1	0.2	0.1	0.1	0.0
Cs	8.1	3.3	8.3	1.5	1.6	1.4	6.9	7.9
Ba	496.6	550.1	386.0	534.0	616.4	545.3	502.2	430.8
La	30.5	32.9	14.8	13.2	15.5	9.8	12.9	24.7
Ce	54.4	61.1	25.0	27.2	32.6	19.6	25.1	66.0
Pr	7.4	9.0	4.8	3.4	4.5	2.8	3.3	7.6
Nd	28.5	38.0	23.5	13.2	18.6	11.7	14.1	28.5
Sm	6.0	8.0	6.8	2.9	3.9	2.4	3.0	6.7
Eu	0.8	0.4	1.8	0.7	0.9	0.6	0.4	1.5
Tb	0.6	1.3	1.1	0.4	0.6	0.4	0.6	1.0
Dy	3.5	8.3	4.9	2.4	3.4	2.3	4.6	4.7
Gd	4.5	7.6	6.1	2.4	3.8	2.2	3.1	5.4
Ho	0.7	1.7	1.0	0.5	0.7	0.5	1.0	1.0
Er	1.7	4.4	2.5	1.3	1.9	1.2	2.8	2.6
Tm	0.3	0.8	0.4	0.2	0.3	0.2	0.5	0.5
Yb	1.9	5.1	2.6	1.6	2.2	1.4	3.4	3.1
Lu	0.3	0.8	0.4	0.3	0.3	0.2	0.5	0.5
Hf	6.2	7.0	4.9	4.6	4.4	5.1	10.9	6.0
Ta	1.2	0.9	0.3	0.4	0.5	0.3	1.1	0.9
Tl	0.4	0.4	0.8	0.2	0.2	0.3	0.3	0.4
Pb	18.4	14.4	7.7	11.5	8.8	7.5	21.1	12.4
Th	10.4	13.3	2.3	3.4	3.6	3.9	6.8	7.6
U	2.5	3.0	0.7	0.8	1.0	1.0	4.1	2.4
LREE	127.7	149.5	76.8	60.7	76.1	46.8	58.9	135.0
HREE	13.4	29.9	18.9	9.2	13.3	8.2	16.5	18.7
REE total	141.1	179.4	95.6	69.8	89.4	55.0	75.4	153.7
(La/Lu)n	0.3	0.3	0.3	0.3	0.3	0.3	0.2	0.3
(La/Sm)n	2.4	1.5	2.4	1.4	1.7	1.6	0.9	1.8
(La/Lu)n	2.8	4.0	4.5	5.3	5.3	5.5	5.6	12.3

Table 1: Trace elemental concentrations of samples of granites and mudstones.

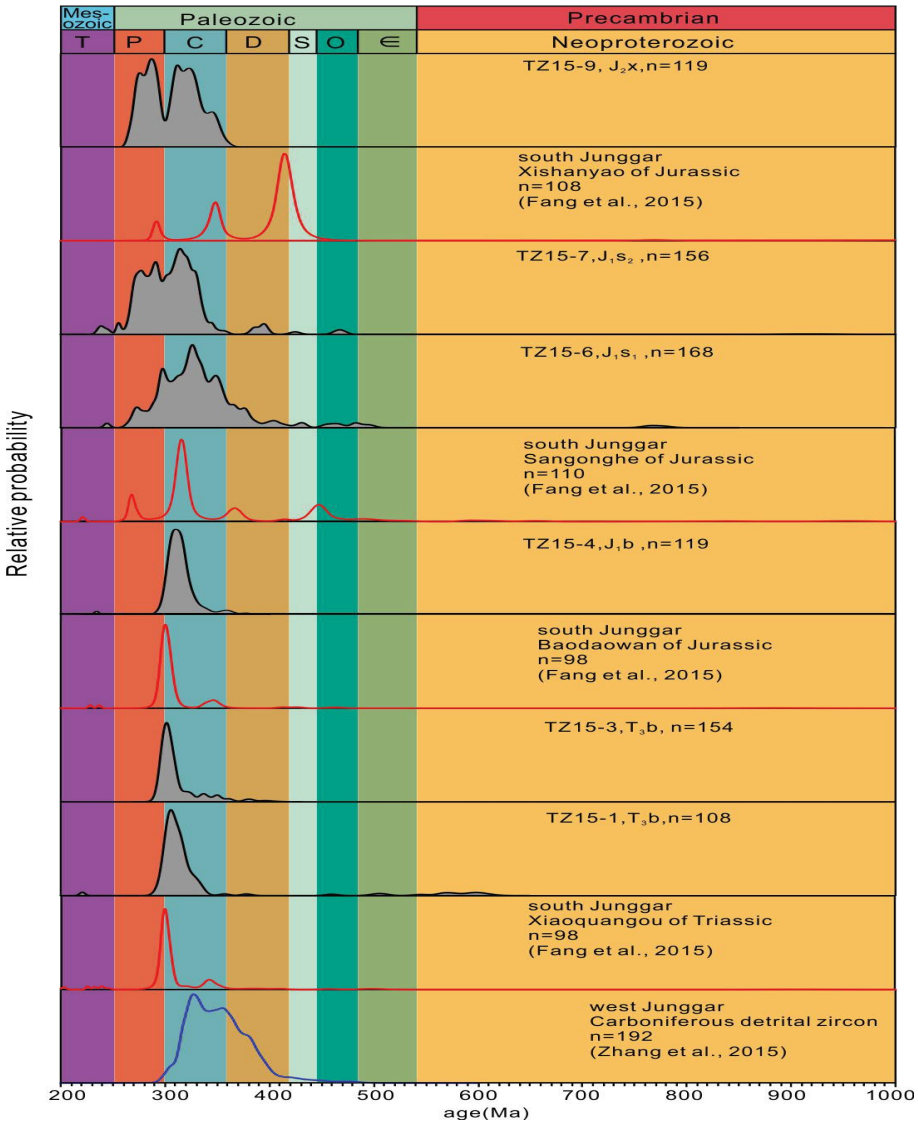

Figure 9: Comparison of detrital Zircon U-Pb probability density distribution plots.

the Jurassic Upper Sangonghe Formation (J_1s^2). The ages of 156 grains range from 238 ± 3 to 471 ± 5 Ma with major peaks at 261-358Ma (92%) (with three peaks at ~277Ma (20%), ~292Ma (17%), ~316 Ma (54%)) and minor clusters at ~240 Ma (2%), ~256 Ma (1%), ~395 Ma (3%) and ~476 Ma (2%).

Sample TZ15-9 is a yellow, medium sandstone collected from the Jurassic Xishanyao Formation. The ages of 119 grains range from 266 ± 3 to 357 ± 6 Ma with major peaks at ~276, ~286, ~312, ~322 and ~345 Ma. The majority of grains are clustered among three groups: 266-295 Ma (42%), 300-336 Ma (46%) and 339-357 Ma (12%).

Results of U-Pb zircon dating of granite and tuff

The U-Pb dates of granitic zircons are shown in Figure 7, Supplementary material. In total, 394 zircon grains, from four volcanic samples, were analyzed. Of those, 358 results are concordant, with ages varying in a broad range between 204 and 470 Ma. These correspond to peaks at ~302 and ~304 Ma.

Sample TZ-1 is a greyish white granite. Out of 126 grains, 119 zircons yielded concordant ages between 289 ± 4 Ma and 352 ± 4 Ma, with $^{207}Pb/^{206}Pb$ ages ranging from 206 ± 36 Ma to 567 ± 97 Ma, and $^{206}Pb/^{238}U$ ages ranging from 289 ± 4 Ma to 352 ± 4 Ma. These zircons define a discordia line with a lower intercept age of 269 ± 21 Ma and an imprecise upper intercept age of 737 ± 220 Ma (MSWD=0.74). The 23 youngest ages have a concordia age of 292.6±9.7 Ma (n=23), with a weighted mean age of 292.5±1.3 Ma. The sequential stage concordia age is 303.3 ± 1.0 Ma (n=63), 317.3 ± 2.0 Ma (n=19), 33.6 ± 4.5 Ma (n=8). A probability map indicates the majority of ages plot at ~302, ~323, ~348, and ~379 Ma (Figure 7).

Sample TZ-2 is a red colored granite collected from the north Karamay pluton. Out of 123 analyzed zircons, 117 grains have concordant ages between 293 ± 4 and 536 ± 10 Ma. The predominant ages are shown by peaks at ~302, ~356, and ~397 Ma. The majority of the 117 grains cluster between 293 and 326 Ma (74%). These zircons define a discordia line with a lower intercept age of 273 ± 20 Ma and an

imprecise upper intercept age of 812 ± 180 Ma (MSWD=0.84). The 65 younger ages have a concordia age of 302.7 ± 1.3 Ma (Figure 7).

Sample SP-2 is greyish white granite collected from a Carboniferous granitic body located at the northern Sanping Reservoir. Of 135 analyses, 115 are concordant showing ages from 288 ± 3 Ma to 384 ± 3 Ma with peaks at ~304, ~325, ~337, and ~360 Ma. These zircons define a discordia line with a lower intercept age of 290 ± 11 Ma and an imprecise upper intercept age of 933 ± 160 Ma (MSWD=0.22). The 14 younger ages have a concordia age of 303.9 ± 2.3 Ma (Figure 7).

Sample SP-1 is a greyish tuff collected from an outcrop near the Sanping reservoir. Of 19 dated grains, seven have dates ranging from 287 ± 5 Ma and 423 ± 5 Ma (Figure 7).

Results of trace elements and rare earth elements

Trace elements and rare earth elements have similar characteristics in the Tuziakeneigou samples except for the TZ-5 claystone. REE concentrations increase from 55 to 179 ppm. Light REE (LREE) concentrations are considerably more enriched than heavy REE (HREE); LREE/HREE ratios vary from 3.57 to 9.51, with $(La/Lu)_n$ = 2.79-12.33. LREE fractionation is more striking than HREE fractionation: $(La/Sm)_n$ = 1.41-3.27 and $(Gd/Lu)_n$ = 0.25-2.00, and HREEs have a concave shape. Negative Eu anomalies vary from 0.17 to 0.84. Similarly, primitive mantle-normalized trace element patterns (Figure 7) are nearly parallel to each other, with significantly negative Ta, Nb, Ce and Ti anomalies (Table 1).

Discussion

Potential sources

Our samples were collected from the Karamay area in the west Junggar adjacent to the northwestern margin of Junggar block, where Silurian to Carboniferous, Jurassic and Quaternary strata are dominant with scarce Permian to early Triassic sedimentary rock exposures (Figure 1). The detrital zircon age spectra of the six samples from Triassic to Jurassic sedimentary rocks share several similar age signatures (Figure 6), such as abundant Paleozoic ages, extremely rare ages between 360 and 1000 Ma, and a majority of grains with Permian and Carboniferous ages. They show a progressive decrease of Mesozoic detrital zircon ages along with a strong increase in later Paleozoic dates from the middle Carboniferous to the middle/lower Permian (Figure 6).

Based on zircon age data (Figure 6), we conclude the provenance of Triassic to Jurassic sediments north of Karamay city changes from a confined local source to mixed multiple sources. Overall, the narrow spectra of dates from the Triassic Baijiantan and Jurassic Badaowan Formations reveal a confined local source that was most likely from the local Karamay granitic plutons northwest of Karamay city with a minor contribution from the recycling of previous sedimentary rocks. Starting with the Jurassic Sangonghe and Xishanyao Formations, broader sources, likely from the northern Karamay granitic plutons and the Sangonghe Formation, may include contributions from the north of the Darbute fault and potentially minor contributions from the southern margin of Junggar Basin.

The Triassic Baijiantan Formation (sample TZ15-1 and samples TZ15-3) has a single, but confined, Late Carboniferous to Early Permian zircon age peak. The samples match well with the west Junggar granite, which mainly formed between 295 and 315 Ma [32]. The youngest age of sample TZ15-1 is 291 ± 4 Ma, which is consistent with the Karamay granitic pluton sample TZ-1 (Figure 7) and previous studies [32,43,44]. In contrast, the Akebasitao granitic pluton, north of the Darbute fault, has a concordia age of 276 ± 5 Ma from seven zircon grain SHRIMP dating [32], is unlikely to be the source of the Baijiantan Formation. Additionally, Sample TZ15-3 shows there are a few grains older than the Carboniferous. These grains could have been recycled from previous sedimentary rocks, such as Ordovician System exposures southwest of Karamay city (Figure 1). The REE characteristics of the Triassic Baijiantan Formation are similar to the Karamay granitic plutons and the Junggar granitic pluton REE (Figure 8), which further confirms that the Baijiantan Formation was likely derived from local granitic plutons. This result is consistent with previous petrographic studies on Triassic Baijiantan Formation clastic rocks that show the majority of lithic fragments are volcanic (acidic magma) [36]. However, this interpretation is not consistent with a previous heavy mineral study of Tuziakeneigou which suggests that they were derived from the northwest Zhayier mountains [45].

The Lower Jurassic Badaowan Formation has a relatively older and broader age distribution than the Triassic samples, but its overall age overlap suggests that the local Karamay granitic plutons remain as main sediment sources for the Jurassic Baodaowan Formation. Starting in the Jurassic, its age distributions are characterized by a relatively broad zircon age spectrum with multiple age peaks, which reveals relatively broader sources than the Triassic samples and the Jurassic Badaowan Formation. The Jurassic Sangonghe Formation (sample TZ15-6 and sample TZ15-7) show a much broader age range than the Triassic Baijiantan Formation and Jurassic Badaowan Formation (Figures. 6 and 9). Besides its main Carboniferous and Middle Permian age peaks, there are some minor Ordovician, Silurian, Devonian and Triassic peaks. The Jurassic Xishanyao Formation (sample TZ15-9) has no grains younger than the Permian and older than the Carboniferous and has a double peak, similar to the Jurassic Sangonghe Formation (sample TZ15-7) (Figure 6).

Previous studies show that the northern Karamay granitic plutons are made up of alkali-feldspar granite, monzonitic granite and granodiorite [43,46,47]. Much broader age ranges have been reported, including 318 ± 5 Ma, 308 ± 5 Ma, 295 ± 6 Ma and 315 ± 6 Ma [32], 315.5 ± 2.8 Ma [43], and 297.6 ± 2. 5 Ma [47] from the north Karamay granitic pluton. The late Carboniferous and early Permian age grains can be derived from granitic plutons at Zhayier Mountain, in which granitic plutons from the northern Karamay granitic pluton and the Hongshan pluton, located to the east of the north Karamay pluton, have ages ranging from ~295 to ~320 Ma (Han et al., 2006). However, the detrital zircon ages of ~270 Ma seen in sample TZ15-7 may come from the Akebastao granitic pluton to the north of the Darbute fault [32]. Devonian to Middle Carboniferous (~420-~320 Ma) zircons may come from Carboniferous sedimentary rocks in the Hatu zone that are located to the north of Darbute fault (Figure 9) [48]. Some older Ordovician and Silurian zircon grains were most likely recycled from previous sedimentary rocks.

There is no known granitic pluton younger than Early Permian, so sources of zircon ages younger than the early Permian are likely recycled from other areas. Compared with zircon age spectra from the Tianshan orogenic belt there is a good match between the Jurassic zircon ages from this study and those from the early Permian to Late Triassic Tianshan orogenic belt [3], especially minor age peaks eg. ~239 Ma and ~256 Ma (Figure 9), which shows that there was a contribution from the Tianshan orogenic belt to the south. Sedimentation in the northwest Junggar Basin may come from the southern margin of Junggar Basin that was influenced by the Tianshan orogen [3].

Triassic to Jurassic sediment dispersal in the northwestern Junggar Basin

Martin [49] interpreted that the Lower to Middle Triassic is characterized by alluvial fan and delta systems that were overlain by lacustrine deposits of the Upper Triassic and, in the Lower-Middle Jurassic, by coal-bearing braided delta systems with main sediment transport from north to south in the basin.

After the Middle Permian, after termination of subduction-accretion processes from the southern west Junggar terrane to the Junggar Basin [50], the Junggar inter-basin steadily received detrital sediments from the basin margins or further. Missing strata from the Permian and Early Triassic, at the edge of Junggar Basin (Figures 1 and 2) [51], suggests that Zhayier Mountain was uplifted as early as the Permian. Angular unconformities and a sedimentary hiatus at the end of Middle and Late Permian were observed at the local [21,52] , which further confirms that Zhayier Mountain, at the northwestern margin of the basin, had been uplifted after the middle Permian.

As discussed earlier, sediments in the Later Triassic Baijiantan Formation to the Jurassic Badaowan Formation were mainly derived from local intrusion granites in the north Karamay plutons at Zhayier Mountain, and there were no sediments transported from north of the Darbute fault to the south. During the Triassic, rejuvenated dextral strike-slip faulting occurred simultaneously with transpressional structures during widespread tectonic reactivation in the CAOB Junggar Basin [53]. Triassic sediment distribution was steady and consequent and lay unconformably on Carboniferous strata in the northwestern margin of Junggar Basin that consisted of mudstones and coarse sandstones.

By the time of Jurassic Sangonghe Formation, the block to the north of the Darbute fault was subducted and uplifted, and the sediment from north of the Darbute fault may have been transported to the northwest Junggar Basin (Figure 9). Sedimentation in the northwestern Junggar Basin experienced a change from a local confined source to much broader multi-direction sources. From the Jurassic Badaowan Formation to the Sangonghe Formation, sedimentary environments were alluvial and braided fans to braided delta front and developed the thick gravels and coarse sandstones of the Badaowan Formation to the medium sandstones of the Sangonghe Formation (Figures 4e and 4f). During the Early-Middle Jurassic, the Junggar Basin, an internally drained basin or walled basin [54,55], and episodic uplifting of the surrounding ranges resulted in episodic folding and reverse faulting in the basin margins.

During the Middle Jurassic, the Xishanyao Formation uncomfortably overlaid the Sangonghe Formation in the Hoxtolgay basin located at the north Zhayier-Halaalate Mountain, and fission track thermo chronology shows the Zhayier Mountain underwent a rapid cooling event during the early Middle Jurassic (178–171Ma) [35,56,57]. These prove that the northern rim of the Junggar Basin, including the northern Zhayier Mountain, were uplifted and subducted. Compared with the Upper Triassic to Lower Jurassic Badaowan Formation, the unimodal distribution of U-Pb ages of the Sangonghe and Xishanyao Formations indicate a widening of the drainage system (Figures 6 and 9). Based on age distributions and variation, we propose that sediments of the Triassic Baijiantan and Jurassic Badaowan sediments were mainly sourced from local granitic plutons. The Jurassic Sangonghe and Xishanyao Formations were derived from the northern Karamay granitic plutons, the areas north of the Darbute fault, with potentially minor contributions from the southern margin of the Junggar Basin.

Conclusions

The main conclusions of this study include

1. Detrital zircon geochronology shows the Triassic Baijiantan Formation and Jurassic Badaowan Formation have relatively confined age distributions. In contrast, the Jurassic Upper Sangonghe and Jurassic Upper Xishanyao Formations demonstrate much broader age ranges.

2. Granitic zircons were mainly formed in the Late Carboniferous-Early Permian with ages ranging from 289 ± 4 Ma to 352 ± 4 Ma, and with concordia ages of 292.6 ± 0.7 Ma, 302.7 ± 1.3 Ma, 317.3 ± 2.0 Ma, 33.6 ± 4.5 Ma.

3. Trace elements and rare earth elements have similar characteristics in the Tuziakeneigou samples except for the TZ-5 claystone. Light REE concentrations are considerably more enriched than heavy REE (HREE). The REE characteristics of the Triassic Baijiantan Formation are similar to those of the Karamay granitic plutons and other west Junggar granitic REEs.

4. Age distributions and variations suggest that sediments of the Triassic Baijiantan and Jurassic Badaowan Formations were mainly derived from local granitic plutons. The Jurassic Sangonghe and Xishanyao Formations were derived from mixed multiple sources, including the northern Karamay granitic plutons, the area north of the Darbute fault, with potentially minor contributions from the southern margin of the Junggar Basin.

Acknowledgements

This study was financially supported by Foundation of Key Laboratory of Mineral Resources in Western China (Gansu Province), Lanzhou University and the Western Doctor Foundation of the Chinese Academy of Sciences, along with Special Funding for Key Laboratories of Gansu Province (1309RTSA041) and Science and Technologic Plan for Jiayuguan City.

References

1. Safonova I (2017) Juvenile versus recycled crust in the Central Asian Orogenic Belt: Implications from ocean plate stratigraphy, blueschist belts and intra-oceanic arcs. Gondwana Research 47: 6-27.

2. Li D, He DF, Qi XF, Zhang NN (2015a) How was the Carboniferous Balkhash-West Junggar remnant ocean filled and closed? Insights from the Well Tacan-1 strata in the Tacheng Basin, NW China. Gondwana Research 27: 342-362.

3. Fang Y, Wu C, Guo Z, Hou K, Dong L, et al. (2015) Provenance of the southern Junggar Basin in the Jurassic: Evidence from detrital zircon geochronology and depositional environments. Sedimentary Geology 315: 47-63.

4. Zhang XR, Zhao GC, Sun M, Eizenhofer PR, Han YG, et al. (2016) Tectonic evolution from subduction to arc-continent collision of the Junggar ocean: Constraints from U-Pb dating and Hf isotopes of detrital zircons from the North Tianshan belt, NW China. GSA Bulletin 128: 644-660.

5. Vincent SJ, Allen MB (2001) Sedimentary record of Mesozoic intracontinental deformation in the eastern Junggar Basin, northwest China: Response to orogeny at the Asian margin. Geological Society of America Memoir 194: 341-360.

6. Xiao Y, Zhang HF, Shi JA, Su BX, Sakyi PA, et al. (2011) Late Paleozoic magmatic record of East Junggar, NW China and its significance: Implication from zircon U-Pb dating and Hf isotope. Gondwana Research 20: 532-542.

7. Zhang JE, Xiao WJ, Han CM, Ao SJ, Yuan C, et al. (2011) Kinematics and age constraints of deformation in a Late Carboniferous accretionary complex in Western Junggar, NW China. Gondwana Research 19: 958-974.

8. Li D, He DF, Santosh M, Ma DL, Tang JY, et al. (2015b) Tectonic framework of the northern Junggar Basin part I: The eastern Luliang Uplift and its link with the East Junggar terrane. Gondwana Research 27: 1089-1109.

9. Yi ZY, Huang BC, Xiao WJ, Yang LK, Qiao QQ, et al. (2015) Paleomagnetic study of Late Paleozoic rocks in the Tacheng Basin of West Junggar (NW

China): Implications for the tectonic evolution of the western Altaids. Gondwana Research 27: 862-877.

10. Liu B, Han BF, Xu Z, Ren R, Zhang JR, et al. (2016) The Cambrian initiation of intra-oceanic subduction in the southern Paleo-Asian Ocean: Further evidence from the Barleik subduction-related metamorphic complex in the West Junggar region, NW China. J of Asian Earth Sci 123: 1-21.
11. Stockmeyer JM, Shaw JH, Brown ND, Rhodes EJ, Richardson PW, et al. (2017) Active thrust sheet deformation over multiple rupture cycles: A quantitative basis for relating terrace folds to fault slip rates. Geological Society of America Bulletin 129: 1337-1356.
12. Yin J, Chen W, Xiao W, Yuan C, Sun M, et al. (2018) Petrogenesis and tectonic implications of early Devonian mafic dike–granite association in the northern West Junggar, NW China. International Geology Review 60: 87-100.
13. Sengor AMC, Natalin B (1996) Paleotectonics of Asia: fragments of a synthesis. Cambridge University Press, Cambridge pp.298-614.
14. Lawrence SR (1990) Aspects of the petroleum geology of the Junggar Basin, Northwest China In: J. Brooks (Ed.), Classic Petroleum Provinces. Geological Society Special Publication pp.545-557.
15. Wu M, Cao J, Wang XL, Tang Y, Wang B, et al. (2014) Hydrocarbon generation potential of Triassic mudstones in the Junggar Basin, northwest China. AAPG Bulletin 98: 1885-1906.
16. Zhou L, Pang X, Wu L, Kuang L, Pang H, et al. (2015) Bottom boundary of deep hydrocarbon accumulation in northwestern margin of Junggar Basin and its identification. Acta Petrolei Sinica 36: 169-175.
17. Li Z, Peng S (2013) U-Pb geochronological records and provenance system analysis of the Mesozoic-Cenozoic sandstone detrital zircons in the northern and southern piedmonts of Tianshan, Northwest China: Responses to intracontinental basin-range evolution. Acta Petrologica Sinica 29: 739-755.
18. Wen H, Jiang Y, Huang H, Liu Y, Wang T, et al. (2016) Provenance and diagenesis of the Upper Jurassic Qigu Formation sandstones in the southern Junggar Basin, NW China. Arabian J of Geosci 9: 1-17.
19. Abulimiti Zou Z, Bao H, Xu Y, Chen L, Yao J, et al. (2012) Provenance analysis of Qingshuihe Formation of Cretaceous in hinterland of Junggar Basin. Xinjiang Petroleum Geology 33: 690-693.
20. Tao H, Wang Q, Yang X, Jiang L (2013) Provenance and tectonic setting of Late Carboniferous clastic rocks in West Junggar, Xinjiang, China: A case from the Hala-alat Mountains. J of Asian Earth Sci 64: 210-222.
21. Bian W, Hornung J, Liu Z, Wang P, Hinderer M, et al. (2010) Sedimentary and palaeoenvironmental evolution of the Junggar Basin, Xinjiang, Northwest China. Palaeobiodiversity and Palaeoenvironments 90: 175-186.
22. Cao J, Wang XL, Sun PA, Zhang YQ, Tang Y, et al. (2012) Geochemistry and origins of natural gases in the central Junggar Basin, northwest China. Organic Geochemistry 53: 166-176.
23. Chen ZL, Liu GD, Wang XL, Gao G, Xiang BL, et al. (2016) Origin and mixing of crude oils in Triassic reservoirs of Mahu slope area in Junggar Basin, NW China: Implication for control on oil distribution in basin having multiple source rocks. Marine and Petroleum Geology 78: 373-389.
24. Jia HB, Ji HC, Li XW, Zhou H, Wang LS, et al. (2016) A retreating fan-delta system in the Northwestern Junggar Basin, northwestern China-Characteristics, evolution and controlling factors. J of Asian Earth Sci 123: 162-177.
25. Kröner A (2015) The Central Asian Orogenic Belt : Geology, Evolution, Tectonics, and Models. Borntraeger Science Publishers pp. 313.
26. Xu XW, Li XH, Jiang N, Li QL, Qu X, et al. (2015) Basement nature and origin of the Junggar terrane: New zircon U-Pb-Hf isotope evidence from Paleozoic rocks and their enclaves. Gondwana Research 28: 288-310.
27. Fang Y, Wu C, Wang Y, Wang L, Guo Z, et al. (2016) Stratigraphic and sedimentary characteristics of the Upper Jurassic-Lower Cretaceous strata in the Junggar Basin, Central Asia: Tectonic and climate implications. Journal of Asian Earth Sciences 129: 294-308.
28. Wu Q (1985) Discussion of the evolution of Junggar Basin Slab, Kazakstan Plate. Xinjiang Petroleum Geology 6: 14-25.
29. Wu Q (1986) An Introduction to developing phase, tectonic province dividing and genesis of local structures of Junggar Basin. Xinjiang Petroleum Geology 7: 31-39.
30. Wang W, Chen Y (2004) Tectonic Evolution and Petroleum Systems in the Junggar Basin. Acta Geologica Sinica 78: 667-675.
31. Watson MP, Hayward AB, Parkinson DN, Zhang ZM (1987) Plate tectonic history, basin development and petroleum source rock deposition onshore China. Marine and Petroleum Geology 4: 205-225.
32. Han B, Ji J, Song B, Chen LH, Zhang L, et al. (2006) Late Paleozoic vertical growth of continental crust around the Junggar Basin, Xingjiang, China (Part 1): Timing of post-collisional plutonism. Acta Petrologica Sinica 22: 1077-1086.
33. Chen J, Han B, Ji J, Zhang L, Xu Z, et al. (2010) Zircon U-Pb ages and tectonic implications of Paleozoic plutons in northern West Junggar, North Xinjiang, China. Lithos 115: 137-152.
34. Windley BF, Alexeiev D, Xiao W, KRO Ner A, Badarch G, et al. (2007) Tectonic models for accretion of the Central Asian Orogenic Belt. J of Geological Soc 164: 31-47.
35. Yang YT, Song CC, He S (2015) Jurassic tectonostratigraphic evolution of the Junggar Basin, NW China: A record of Mesozoic intraplate deformation in Central Asia. Tectonics 34: 86-115.
36. Gu X, Liu Y, Kuang H, Cen C, Li J, et al. (2010) Sedimentation and reservoir characteristics of Middle Triassic-Lower Jurassic oil and deposits at Tuziakeneigou of northwester Junggar Basin. Acta Petrologica et Mineralogica 30: 215-224.
37. Xie X, Cains W, Manger WL (2016a) U–Pb detrital zircon evidence of transcontinental sediment dispersal: provenance of Late Mississippian Wedington Sandstone member, NW Arkansas. International Geology Review 58: 1951-1966.
38. Xie X, O'Connor PM, Alsleben H (2016b) Carboniferous sediment dispersal in the Appalachian–Ouachita juncture: Provenance of selected late Mississippian sandstones in the Black Warrior Basin, Mississippi, United States. Sedimentary Geology 342: 191-201.
39. Shaanan U, Rosenbaum G (2016) Detrital zircons as palaeodrainage indicators: Insights into southeastern Gondwana from Permian basins in eastern Australia. Basin Research 1-12.
40. Gehrels GE, Blakey R, Karlstrom KE, Timmons JM, Dickinson B, et al. (2011) Detrital zircon U-Pb geochronology of Paleozoic strata in the Grand Canyon, Arizona. Lithosphere 3: 183-200.
41. Ludwig KR (1998) On the treatment of concordant uranium–lead ages. Geochimica et Cosmochimica Acta 62: 665-676.
42. Lin S, He M, Hu S, Yuan H, Gao S, et al. (2000) Precise determination of trace elements in geological samples by icp-ms using compromise congditions and fine matrix matching strategy-lin-analytical sciecnces. Analytical Sciences 16: 1291-1296.
43. He J, Chen B (2011) Petrogenesis of Karamay plutons in the west Junggar: Constraints from geochromology, petrology and geochemistry. Earth Science Frontiers 18: 191-211.
44. Yang G, Li Y, Santosh M, Yang B, Zhang B, et al. (2013) Geochronology and geochemistry of basalts from the Karamay ophiolitic melange in West Junggar (NW China): Implications for Devonian-Carboniferous intra-oceanic accretionary tectonics of the southern Altaids. GSA Bulletin 125: 401-419.
45. He M, Zhang L, Yao J, Li S, Li Q, et al. (2017) Heavy Mineral Characteristics and Their Implication for Provenance of the Middle to Upper Triassic on the Northwest Margin of Junggar Basin, North China. Earth Science Research 6: 65-75.
46. Tang GJ, Wang Q, Wyman DA, Li ZX, Zhao ZH, et al. (2012) Late Carboniferous high εNd (t)–εHf (t) granitoids, enclaves and dikes in western Junggar, NW China: Ridge-subduction-related magmatism and crustal growth. Lithos 140-141: 86-102.
47. Li Y, Li G, Kang L, He X, Zhang H, et al. (2013) Evidence of zircon U-Pb geochronology for magma mixing of Xiaerpu granite in West Junggar. Acta Petrolica Sinica 29: 3023-3030.
48. Zhang L, Wang G, Gao R, Shen, T, Zong R, et al. (2015) U-Pb Chronology of Detrital Zircons from the Carboniferous Sequences and its Geological Implications in West Junggar. Geotectonica et Metallogenia 39: 704-717.
49. Martin T, Sun G, Mosbrugger V (2010) Triassic-Jurassic biodiversity, ecosystems, and climate in the Junggar Basin, Xinjiang, Northwest China. Palaeobiodiversity and Palaeoenvironments 90: 171-173.

50. Li D, He D, Lian Y, Lu Y, Yi Z (2016) Structural evolution and late Carboniferous magmatism of the Zhongguai arc in the western Junggar Basin, Northwest China: implications for tectonic evolution of the Junggar Ocean. International Geology Review 59: 1234-1255.

51. XBGMR (1965) Geological map of Karamay region. Geological map of Karamay region, 1:200,000. Xinjiang Bureau of Geology and Mineral Resources, China.

52. He M, Jin Z, Li T, Guo X, Yang T, et al. (2014) Stratigraphic framework and microfacies of the Triassic Lower Karamay Formation in districts I, III, NW Junggar, China. J of Earth Sci 25: 1003-1017.

53. Allen MB, Vincent SJ (1997) Fault reactivation in the Junggar region, northwest China: the role of basement structures during Mesozoic-Cenozoic compression. Journal of the Geological Society 154: 151-155.

54. Sobel ER, Hilley GE, Strecker MR (2003) Formation of internally drained contractional basins by aridity-limited bedrock incision. Journal of Geophysical Research Solid Earth 108: 1-23.

55. Carroll AR, Graham SA, Smith ME (2010) Walled sedimentary basins of China. Basin Research 22: 17-32.

56. Guo ZJ, Zhang ZC, Wu CD, Fang SH, Zhang R, et al. (2006) The Mesozoic and Cenozoic Exhumation History of Tianshan and Comparative Studies to the Junggar and Altai Mountains. Acta Geologica Sinica 80: 1-15.

57. Yuan W, Zheng Q, Bao Z, Dong J, Carter A, et al. (2009) Zircon fission track thermochronology constraints on mineralization epochs in Altai Mountains, northern Xinjiang, China. Radiation Measurements 44: 950-954.